An injectable and self-healing hydrogel for spatiotemporal protein release via fragmentation after passing through needles

Cho, Ik Sung

Ooya, Tooru

(Citation)
Journal of Biomaterials Science, Polymer Edition,29(2):145-159

(Issue Date)
2018

(Resource Type)
journal article

(Version)
Accepted Manuscript

An Injectable and Self-Healing Hydrogel for Spatiotemporal Protein Release via Fragmentation After Passing Through Needles

Ik Sung Cho[a] and Tooru Ooya[a]*

[a]*Department of Chemical Science and Engineering, Graduate School of Engineering, Kobe University, Kobe, Japan*

*To whom correspondence should be addressed;

E-mail: ooya@tiger.kobe-u.ac.jp

Tel.: +81-78-803-6255; Fax: +81-78-803-6255.

An Injectable and Self-Healing Hydrogel for Spatiotemporal Protein Release via Fragmentation After Passing Through Needles

A dynamic hydrogel formulated by mixing a glycol chitosan (GC) and an oxidized dextran (Odex) were studied for protein-controlled release in conjunction with the hydrogel fragmentation. A series of injectable dynamic hydrogels were derived from GC and Odex upon simple mixing without the addition of chemical crosslinking agents. The gelation readily took place at physiological pH and temperature. The influence of the concentration of GC and Odex on the gelation time, mechanical properties, water content, in vitro degradation were investigated. The Odex/GC hydrogels showed good self-healing ability under physiological conditions and kept the dynamic Schiff-base linkage at over 2 wt%. The release kinetics of a model protein (bovine serum albumin) was found to be controlled by changing the needle size upon injection, attributed to modulation of apparent size and shape of the fragmented hydrogels even in the self-healed state. Therefore, the GC-based injectable and dynamic hydrogels are expected to be a promising platform for protein delivery system and various biomedical applications.

Keywords: Injectable, Self-healing hydrogel, Carbohydrates, Schiff-base, Protein delivery

Introduction

Hydrogels have been an issue of extensively research in the past decades and their properties such as biocompatible properties, high water content, easy control of solution transport, soft and elastic properties make them very attractive for biomedical application [1-3]. Among them, the injectable hydrogels have received much attention and studied for various biomedical applications, so that this system could fill irregular shaped defects and remain at the desired position by implanting into tissues through a minimally invasive strategy [4,5]. From this advantage, they could provide patient-compliance better than physical surgery [6], and thus, injectable hydrogels have attracted much attention for their potential applications for scaffolds for tissue engineering [7] and drug delivery [8]. So far,

many injectable hydrogels have been successfully investigated: The typical characteristic is that the hydrogels are injected as a liquid, followed by gelation in response to physical/chemical conditions at the injected sites [9-13]. However, these traditional injectable hydrogels are produced through rapid changes in environmental conditions or use of some toxic organic reagents, which often causes uncontrollable gelation processes and limited *in vivo* applications. Meanwhile, the slow gelation causes loss of the encapsulated cells or drugs and diffusion from the target site, while an extremely rapid gelling process results in needle clogging and delivery failure [14,15].

As a new type of biocompatible material, dynamic hydrogels have been developed as an alternative to the traditional injectable hydrogels. Unlike the traditional injectable hydrogels, injectable dynamic hydrogels could homogeneously encapsulate pharmaceutical drugs/cells *in vitro* under physiological condition and has the ability to be injected after gelation. In addition, the hydrogels could be squeezed and pushed through a needle as solid hydrogel fragments, then recovered and self-heal into an integral hydrogel at the target site under physiological conditions without external stimuli [16-18]. This system allows for easy administration and higher therapeutic activity of drugs and cells by preventing the needle clogging with rapid gelation and avoiding the potential risk of drugs/cells loss during the injection [19]. There are some reports about the injectable self-healing hydrogels [17,20,21]. However, they still have several limitations of their own, including alkali environment (pH 8) to form a hydrogel, a UV irradiation is required after being injected, or a long time is required for self-healing (3 h).

Herein, we focused on an injectable and dynamic hydrogel derived from combination of glycol chitosan (GC) and dextran based on Schiff-base chemistry. Chitosan, one of the polysaccharides, has been confirmed to be biocompatible and biodegradable [22,23]. It has been extensively investigated for in pharmaceutical,

cosmetics and biomedical applications [24]. However, chitosan is hardly soluble in physiological conditions and can just dissolved in acid condition. On the contrary, glycol chitosan (GC), a water-soluble chitosan derivative, has good solubility in water and the free amine groups would remain unaffected, letting for future modification [25,26]. Also, dextran is a naturally occurring bacterial polysaccharide that is biodegradable and biocompatible and has been used as a macromolecular carrier for of drugs or proteins delivery and for separation and purification of biological materials [27]. It is a classic method to functionalize dextran to oxidized dextran using sodium periodate and form a pair of aldehyde groups that could act as a macromolecular crosslinker agent for those polymers bearing free amino groups to form hydrogels by Schiff-base reaction that is advantageous in terms of a controllable reaction rate by changing of the medium pH [28-31]. Several oxidized dextran (Odex)-based hydrogels have been developed with *N*-carboxyethyl chitosan, quaternized chitosan or chitosan hydrochloride as a conventional injectable hydrogel by taking advantage of the *in-situ* gel formation feature of the reversible Schiff-base linkage for wound dressing, and cell scaffolds [30,32,33]. In addition, the hydrogels formed by Schiff-base reaction have been exploited to deliver proteins: The long term sustained release of bioactive proteins was achieved, keeping with their biological activities [34,35]. However, the protein release kinetics after the injection of the hydrogels were still unclear.

In this study, we have paid attention to not only the injectable and dynamic properties of the *in situ*-generated hydrogels but also needle size-dependent fragmentation of hydrogels and the influence toward protein release kinetics. When the hydrogels are injected by passing through needles for injection, the size of fragmented hydrogels can be controlled by changing needle size, because the controlled release of proteins is known to be strongly dependent on the hydrogel shapes such as sphere,

cylinder and slab [36]. By passing through needles, shapes of the fragmented hydrogels might be varied, which is possibly alter the release kinetics. Recently, dynamic and injectable hydrogels have been focused on controlled release of biologically active agents such as pH-responsive and tumour-specific drug release [37] and spatiotemporally controlled release of a recombinant Rho-inhibiting C3 toxin [38].

The aim of this work is to evaluate a series of injectable and dynamic hydrogels based on GC and Odex for protein release. The hydrogels were prepared by Schiff-base reaction between the amino group of GC and aldehyde group of Odex under physiological condition. Various characteristics of hydrogels, including concentration dependency of gelation kinetics, mechanical property, swelling ratio, degradation behaviour, and self-healing capability were investigated. A model protein, bovine serum albumin (BSA), was loaded in the hydrogels, and release behaviour of BSA from the hydrogels after passing through different size of needles was discussed.

Experimental

Materials

Glycol chitosan (GC, D DP≥200, degree of acetylation = 9.13 ± 0.89% as determined by ^{1}H-NMR), diethylene glycol, albumin from bovine serum (BSA) and acetone were purchased from Wako Pure Chemical Industries, Ltd (Osaka, Japan). Dextran (Dex, M_n=50,000-70,000), sodium periodate, sodium cyanoborohydride and fluorescein isothiocyanate isomer I (FITC) were purchased from Nacalai tesque (Kyoto, Japan). *Tert*-butyl carbazate was purchased from Tokyo Chemical Industry Co., Ltd (Tokyo, Japan).

Preparation of oxidized dextran

Oxidized dextran (Odex) was prepared by first dissolving 2 g of Dex in 160 mL of distilled water, followed by the dropwise addition of 1.03g of $NaIO_4$ dissolved in 40 mL of distilled water. This mixture was stirred at room temperature for 24 h. After the reaction, an equimolar amount of diethylene glycol was added to quench the unreacted $NaIO_4$ and stirred for 1 h. The Odex mixture was then dialyzed against distilled water for 1 day using a dialysis membrane (MWCO 6,000-8,000), and the pure Odex was obtained as a powder state after lyophilization (yield 65%). The oxidation degree of Odex was determined by quantifying the aldehyde groups formed by tert-butyl carbazate via carbazone formation [32].

Briefly, an Odex solution (10 mg/mL in an acetate buffer at pH 5.2) was prepared, and then a five-fold excess *tert*-butyl carbazate in the same buffer was added. The mixture was allowed to react for 24 h at room temperature after that five-fold excess of $NaBH_3CN$ was added. After another 12 h, the reaction product was precipitated thrice with acetone and the final precipitate was dialyzed thoroughly against water followed by lyophilization. The degree of oxidation was assessed by ^{1}H-NMR by integrating the peaks at 1.3 ppm (*tert*-butyl) against 4.8 ppm (anomeric proton of dextran). The oxidation degree of dextran was determined to be 33%.

Characterization

The chemical compositions of GC, Dex, and Odex were characterized by ^{1}H NMR spectroscopy using a JEOL ECS 400 NMR (JEOL, Japan) operating at 400 MHz. The polymer samples were dissolved in D_2O (10 mg/mL). The residual H_2O peak in D_2O was used as a reference peak at δ 4.65. The FT-IR spectra of GC, Odex, and Odex/GC hydrogel were recoded using a FT-IR apparatus (FT-IR-460 plus, JASCO, Japan) in the range of 4000-500 cm^{-1}.

Preparation of Odex/GC solutions and hydrogels

Aqueous Odex and GC solutions of 1, 2, and 3 wt % in 0.01M PBS (pH 7.4) were prepared, respectively, and stored at 4 ^{o}C before use. To prepare hydrogels 1, 2, and 3 wt % Odex solutions were mixed with 1, 2, and 3 wt % GC solutions in a ratio of 1:1, respectively. The mixtures were gently stirred for 10s and the mixture was maintained at 37 ^{o}C for gelation. The final hydrogels were marked as Odex/GC 1, Odex/GC 2, and Odex/GC 3, respectively. The gelation time of the Odex/GC hydrogels were observed by the tube inverting method. All the gelation times were measured in triplicate for each.

Rheological measurements of the hydrogels

The rheological behaviors of Odex/GC hydrogels with different concentrations of polymer were investigated at 37 ^{o}C by using a rheometer (MCR-302, Anton Paar, Austria) with 20 mm stainless-steel parallel plates. The Odex/GC hydrogels with gelation time of 12 h, were applied to the rheometer, and storage modulus (G`) and loss modulus (G``) were determined as a function of the frequency. A dynamic frequency sweep tests with frequency ranging from 0.1 to 10 Hz at 0.1 % shear rate were performed.

Water content of the hydrogels

For water content analysis, the Odex/GC hydrogels with different polymer concentration (1, 2, 3 wt %) were made as disks (diameter of 10 mm and height of 5 mm). These hydrogels were immersed into distilled water at 37 ^{o}C for 24 h and then weighed after careful removal of excess PBS. The freeze-dried gels were also weighed separately. All experiments were carried out in triplicate. The water content of the hydrogels was calculated using in the following equation (1).

$$\text{Water content} = \frac{M_{wet} - M_{dry}}{M_{dry}} \quad (1)$$

where M_{wet} is wet hydrogel weight, and M_{dry} is the dry hydrogel weight.

In vitro degradation

In order to evaluate the degradability of the hydrogels, *in vitro* degradation tests were carried out. Briefly, different groups of hydrogels with similar size and shape were immersed into 0.01M PBS (pH 7.4) at 37 ^{o}C. Weight loss of initially weighed hydrogels (M_i) was monitored as a function of incubation time. At specified time intervals, hydrogels were removed from 0.1M PBS and weighed (M_t). The *in vitro* degradation of the hydrogels was calculated using in the following equation (2).

$$\text{Mass loss (\%)} = \frac{M_t}{M_i} \times 100 \quad (2)$$

Morphological studies

The morphological structures of the hydrogels were examined by using a scanning electron microscope (JSM-6510, JEOL, Japan). The hydrogel samples were frozen in liquid nitrogen and freeze-dried. The dried samples were fractured to expose cross-sections of the hydrogel.

Injectable and self-healing test of Odex/GC hydrogel

The self-healing behaviors of the hydrogels were analyzed both microscopy and quantitative methods using the Odex/GC 2 as an example. In the microscopy method, hydrogel was put into syringes and injected through a 23-gauge needle into cylindrical shape mold and cultured for 30 min at 25 ^{o}C without any external intervention. The newly formed cylindrical shape hydrogels were taken out from the mold and immersed in distilled water. The stability was assessed by gently shaking and inverting the vials [17,39]. In a quantitative way, the Odex/GC 2 hydrogel with gelation time of 12 h as well as the dynamic hydrogel with healing time of 30 min and 2 h after injection, and dynamic

frequency sweep test with frequency ranging from 0.1 to 10 Hz, were performed at 37 ºC under a fixed strain at 0.1 %.

Cell viability test

To evaluate the viability of cells cultured with GC and Odex, 3-(4,5-dimethylthiazol-2-yl)-2,5-diphenyltetrazolium bromide (MTT) assay was performed. The NIH 3T3 cells were seeded in a 96-well plate (5×10^3 cells/well) and incubated at 37 ºC and 5% CO_2 for 24 h. The cells were incubated with various concentration of GC and Odex (0.5, 1.0, 2.0 mg/mL), the cells were incubated for 1 day at 37 ºC. The MTT solution (10 μL) was added to each well. After incubation for 2 h at 37 ºC, the optical intensity was then measured by using a microplate reader (SH-9000, CORONA ELECTRIC, Japan). The experiments were performed in triplicate.

Protein loading and in vitro protein release studies after passing through needles

To study the release behavior of a model protein, Odex/GC 2 hydrogel loaded with 1 wt % of FITC-bovine serum albumin (BSA) were prepared. A FITC-BSA-encapsulated hydrogel was put into syringes and injected through 23, 20, 18-gauge needles into mold for 2 h at 25 ºC. The final hydrogels were marked as GEL-23G, GEL-20G, and GEL-18G, respectively. Each hydrogel was placed in 15 mL of PBS solution at 37 ºC. At fixed time interval, 1 mL of the release medium was withdrawn and replaced immediately with fresh buffer. The protein content was determined by a emission intensity of FITC at 519 nm (Excitation at 493 nm). All experiments were performed in triplicate.

Results and discussion

Preparation and characterization of Odex/GC hydrogels

The Odex was simply prepared using sodium periodate. The oxidized dextran bearing aldehyde groups serves as a good macromolecular crosslinker that can reversible crosslink with polysaccharides bearing free amino groups. The representative ^{1}H NMR spectra of GC, Dex, Odex were shown in Figure 1a. The peaks appeared at 2.65 ppm and 3.2-4.0 ppm on the ^{1}H NMR spectra of GC, which was attributed to the primary amine residue and the protons of the glucopyranosyl ring, respectively. The peak at 2.0 ppm arosed from the protons of methyl protons of the acetyl group in GC. Based on these assignments, the content of free amine groups of the GC was calculated as 91 % by comparing the integrated signal area of the protons of the glucopyranosyl ring with those of the acetyl group. Also, as compared with the spectra of Dex and Odex, some additional peaks in the range of 4.2-5.8 ppm assigned to the protons from the hemiacetal structures were observed [40]. Figure 1b showed the FT-IR spectra of GC, Dex, Odex, and Odex/GC hydrogels. An absorption peaks of the aldehyde groups (C=O) in Odex appeared at 1,725 cm^{-1}, compared with that of Dex. The peak of aldehyde was not conspicuous, which is due to hemiacetal formation of free aldehyde groups. A characteristic peak at 1,598 cm^{-1} was attributed to the amino group ($-NH_2$) bending vibration of GC. In the spectrum of the Odex/GC hydrogel, the characteristic absorption band of the newly formed Schiff-base linkage (-C=N-) at 1,604 cm^{-1} was confirmed, suggesting that the coupling reaction was occurred between -CHO of Odex and $-NH_2$ of GC [33].

Transparent Odex/GC hydrogels were formed by homogeneously mixing Odex and GC dissolved in 0.01 M PBS (pH 7.4) at 37 ^{o}C (Figure 2). The formation of hydrogels was attributed to the Schiff-base reaction between the amine groups on GC and aldehyde groups along the Odex molecular chains, as mentioned in Figure 2. The gelation time was

determined at 37 ^{o}C, and the results were shown in Table 1. The gelation time of the Odex/GC hydrogels decreased with increasing polymer concentration. Odex/GC 1 showed the longest gelation time (231 ± 10 s). With increasing the polymer concentration from 2 to 3 wt %, the gelation time decreased to 114 ± 4 and 42 ± 3 s for Odex/GC 2, and Odex/GC 3, respectively. This result indicates that the high Odex/GC concentration increased the chances of an encounter of reactive groups (amino and aldehyde) on polymer chains and thus increased the probability of reaction among these groups.

Rheological behaviour of Odex/GC hydrogels

The mechanical properties of Odex/GC hydrogels were determined by an oscillatory rheology experiments at 37 ^{o}C. Figure 3a presented the storage modulus G` and loss modulus G`` of the hydrogels as a function of frequency at fixed strain of 0.1 %. It is known that G` is the elastic part of the hydrogel, while G`` corresponds to the viscous part. The G` of all hydrogels were found to be greater than the G`` over the entire range of frequency, indicating that the all hydrogels are more elastic than viscous. The value of G` increased with an increase in polymer concentration from 1 to 3 %, indicating that the increased Odex/GC concentration contributed to a significant increase in storage modulus, due to a higher crosslinking density resulting from the higher concentration of reactive.

In vitro biodegradation

The *in vitro* degradability of the Odex/GC hydrogels was monitored by examining the weight loss of hydrogels with interval time in 0.01 M PBS (pH 7.4) at 37 ^{o}C. As shown in Figure 3b, all the hydrogels (Odex/GC 1, Odex/GC 2, and Odex/GC 3) underwent mass loss for the first 5 days, after that a more gradual degradation proceeded implying that the degradation of the hydrogels can be attributed to the hydrolytic susceptibility of Schiff-base linkage [32]. At over 2 wt% of Odex/GC concentration, the hydrolytic susceptibility

seemed to be suppressed. At day 14, the weight remaining ratio of Odex/GC 1, Odex/GC 2, and Odex/GC 3 hydrogels was 18.7%, 55.4%, and 57.2 %, respectively. These results suggest that the hydrolytic susceptibility of Schiff-base linkage and/or untying the polymer network could be controlled by the feed concentration between 1 and 2 wt%. One of the considerable reasons is the correlation of the crosslinking density, as mentioned in Figure 3a: Polymer network with high crosslink density in Odex/GC 2 and Odex/GC 3 hydrogels exhibited large amount of crosslinked points (i.e.; Schiff-base linkage), although the crosslink density of Odex/GC 1 hydrogel was much lower than that of the others. Therefore, the hydrolytic susceptibility of Schiff-base linkage is likely to be governed by the crosslink density. Alternatively, even if the rate of Schiff-base cleavage was the same between all the hydrogels, the high chain entanglements that was attributed to the high crosslink density of Odex/GC 2 and Odex/GC 3 hydrogels led to slow mass loss [41].

Water content and morphology of the hydrogels

The water content of the Odex/GC hydrogels in distilled water was measured at 37 ºC. and was found to be dependent on the polymer concentration: As shown in Figure 4a, the water content decreased rapidly from 28.1 to 10.3 with an increase in the Odex/GC concentration 1 to 3 wt%. This result was well consistent with the rheological data (Fig 3a).

The SEM images of the hydrogels were shown in Figure 4b-d. All the hydrogels exhibited a continuous and highly porous structure. The Odex/GC 1, Odex/GC 2, and Odex/GC 3 showed microporous structure with pore size of 50, 22.2, and 8.3 μm, respectively. The results of SEM images indicate the smaller three-dimensional net-hole with increasing the Odex/GC concentration, and the results were in good agreement with the data of water content (Figure 4a). These were attributable to a higher crosslinking

density with higher concentration of Odex/GC. Therefore, these porous and interconnected structural features of the matrices could be easily modulated by just chaining the concentration of Odex/GC, leading to the changing amount of water as well as allowing easier solvent uptake.

Self-healing behaviour and mechanical recovery of the Odex/GC hydrogels

Considering the dynamic Schiff-base crosslinks existed in the hydrogel networks, the Odex/GC hydrogels are expected to be injected from syringes through needles into the target sites. To test both the injectability and self-healing ability, Odex/GC 2 hydrogels were tested as a model hydrogel. The hydrogel disc was put into a 23-gauge syringe and extruded through a needle into cylindrical mold or donut shape (Figure 5a, b). After that, the molds filled the hydrogel fragments were left at room temperature for 30 min without any external interventions, the hydrogel fragments self-healed via dynamic Schiff-base linkage and turned into dense hydrogels with the cylindrical and donut shape (Figure 5c). The self-healed hydrogels were stable when exposed to gentle shaking and inverting of the vials filled with 0.01M PBS (pH 7.4) (Figure 5d, e). These tests demonstrated good injectability and the self-healing properties of the Odex/GC hydrogels, thus enabling the construction of three-dimensional architecture [42].

To assess the mechanical properties of the self-healed Odex/GC hydrogels after the injection, we performed the rheological measurements as a function of frequency (0.1-10 Hz) at fixed strain of 0.1 % under three different conditions: The first one was sample of original hydrogel, which was directly prepared by mixing Odex and GC solution in a cylindrical mold, followed by standing for 12 h for gelation. The second one was a self-healed fragment obtained after injected into a cylindrical mold, followed by standing for 120 min at 25 ^{o}C. The third one was the same as the second one, but that was stand for 30 min at 25 ^{o}C. As shown in Figure 6a, G` of the self-healed hydrogels obtained after

standing for 30 and 120 min showed 274 Pa and 311 Pa, respectively. These values are close to that of the original hydrogel (393 Pa), meaning that the self-healed hydrogel was calculated to be recovered by 79 % storage modulus at 120 min healing time. As shown in Figure 6b and c, cross-section of the SEM pictures also supported the results of Figure 6a: There was no significant difference between the original hydrogel and the self-healing hydrogels, although the seam was still visible. These results indicate that the elasticity of the original hydrogel was completely recovered even after passing through the needle for the injection, and therefore, the injectability of the dynamic hydrogels could provide uniform distributions of cargos (i.e. drug/cell etc.) and more controllable placement of hydrogels [17].

In vitro viability

It is known that the cytotoxicity of biomaterials is extremely important for their future applications. The cytotoxicity of GC and Odex was determined by an MTT assay as shown in Figure 7. Cytotoxicity of the GC and Odex against NIH3T3 was found to be very low even at high concentration (2 mg/mL) over the culture time. These results indicate that both the components of the hydrogels have no apparent cytotoxicity.

Protein loading and release

In order to investigate whether the release of the encapsulated protein can be controlled by the different size of the needle for injection or not, a model protein, BSA, which was also fluorescently labeled with FITC, was loaded into the Odex/GC 2 hydrogel just mixing together with Odex and GC. In addition, if FITC-BSA is dispersed uniformly throughout the hydrogel matrix, we can assume that the FITC-BSA-loaded Odex/GC 2 hydrogel acts as a monolithic device, where the loaded protein can diffuse from the device rapidly relative to the hydrolytic degradation of the matrix [43]. Since the size and shape

of hydrogels such as slab, sphere and cylinder affect the release kinetics [44], the fragmented size of the self-healed hydrogels after passing through the 23, 20, 18-gauge needles are thought to be one of the key factors for controlled release.

The release behavior of FITC-BSA from the GEL-23G, 20G and 18G in 0.01 M PBS (pH 7.4) at 37^{o}C were shown in Figure 8a. An initial burst up to 18-22% of the loaded FITC-BSA was found in all the self-healed hydrogel within 1 day. This phenomenon is likely to be due to the dissociation of weakly absorbed protein on the hydrogel surface [45]. And then the residual FITC-BSA was slowly released 12 days. The final BSA released from the hydrogels is 35.4 ± 0.4%, 32.1 ± 0.9%, and 29.4 ± 0.8% for GEL-23G, GEL-20G, and GEL-18G, respectively. These results suggest that a part of FITC-BSA was entrapped in the hydrogels despite of the needle size because of Schiff-base formation between the amino groups of BSA and the aldehyde of Odex. The release of FITC-BSA from GEL-23G seems to be fast as compared to release from GEL-20G and 18G during the release span (for 12 days). To further understand the difference, the release profiles of FITC-BSA were estimated by non-steady diffusion mechanism from cylinder-shaped monolithic solutions[43]. The release of drugs from a cylinder is expressed as follows:

$$\frac{M_t}{M_0} \times 100 = 4\left(\frac{Dt}{r^2\pi}\right) - \frac{Dt}{r^2} \qquad (3)$$

where M_0 is total amount of drug loaded, M_t, is the amount released at time t, r is the radius of the cylinder, and D is the diffusion coefficient. Here, r of GEL-23G, GEL-20G, and GEL-18G was 0.064, 0.089, and 0.125 cm, respectively. An initial time showing the burst release (0-24 h) was eliminated, and the curve fitting for the cylinder was carried out after 24 h. The results of the modelling analysis for the release of FITC-BSA from the fragmented and self-healed Odex/GC 2 were shown in Figure 8b. By curve fitting the

release profiles of FITC-BSA during 12 days (288 h) using Origin 8.0J software, those profiles did not follow the release from a cylinder; the diffusion seemed to be faster than the expected diffusion based on the cylinder-based equation. If the fragmented particle size of the polymer is distributed, the polydispersed particles generally cause a substantial acceleration of the transport at early times. Therefore, the accelerated properties in Figure 8b suggests that the passing the hydrogel through the needles distributed the size of fragments. In addition, if we supposed that BSA release follows the cylinder model, the *D* value increased from 2.05 x 10^{-6} to 7.35 x 10^{-7} (cm^2/h) as the needle size decreased from 18-gauge to 23-gauge. This result demonstrated that the needle size was found to affect the drug release efficiency. The effect of the composition on the release rate can be explained by the difference in the size of the needles used at the time of injection. As shown in Figure 8c-e, the smaller the size of the needles is, the smaller hydrogel fragments observed, which presented more boundaries to be found in dynamic hydrogel. In addition, as mentioned before in Figure 6b and 6c (SEM images of the original and the self-healed ones), the roughness of the hydrogel matrix after the self-healing tends to increase. This observation suggest that the boundaries generated by the needle-size-dependent hydrogel fragments increase the surface area of the hydrogel, resulting in increasing the apparent release rate of FITC-BSA.

Conclusion

A dynamic hydrogel was prepared from glycol chitosan and oxidized dextran via Schiff base linkage. The gelation time, mechanical properties, degradation profile, water content, pore size and the self-healing capability were easily modulated. BSA was easily loaded in the hydrogel by just mixing two kinds of precursor's dextran and glycol chitosan solution, and the release kinetics of BSA was accelerated by passing through changing

needle size. Therefore, the dynamic hydrogels can be developed for injectable and spatiotemporal protein delivery.

Acknowledgements

This work was supported by a Grant-in-Aid for JSPS Research Fellow (JSPS KAKENHI Grant Number 17J09992) and a Grant-in-Aid for Scientific Research on Innovative Areas "New Polymeric Materials Based on Element-Blocks (No.2401)" (JSPS KAKENHI Grant Number JP15H00748).

Reference

1. Slaughter BV, Khurshid SS, Fisher OZ, et al. Hydrogels in regenerative medicine. Adv Mater. 2009;21(32-33):3307-3329.
2. Hoffman AS. Hydrogels for biomedical applications. Adv Drug Deliv Rev. 2012;64:18-23.
3. Lee KY, Mooney DJ. Hydrogels for tissue engineering. Chem Rev. 2001;101(7):1869-1880.
4. Li L, Yan B, Yang J, et al. Novel Mussel-Inspired Injectable Self-Healing Hydrogel with Anti-Biofouling Property. Adv Mater. 2015;27(7):1294-1299.
5. Jeong B, Bae YH, Kim SW. Drug release from biodegradable injectable thermosensitive hydrogel of PEG–PLGA–PEG triblock copolymers. J Control Release. 2000;63(1):155-163.
6. Moon HJ, Park MH, Joo MK, et al. Temperature-responsive compounds as in situ gelling biomedical materials. Chem Soc Rev. 2012;41(14):4860-4883.
7. Park H, Guo X, Temenoff JS, et al. Effect of swelling ratio of injectable hydrogel composites on chondrogenic differentiation of encapsulated rabbit marrow mesenchymal stem cells in vitro. Biomacromolecules. 2009;10(3):541-546.

8. Huynh DP, Nguyen MK, Pi BS, et al. Functionalized injectable hydrogels for controlled insulin delivery. Biomaterials. 2008;29(16):2527-2534.
9. Zhu W, Ding J. Synthesis and characterization of a redox-initiated, injectable, biodegradable hydrogel. J Appl Polym Sci. 2006;99(5):2375-2383.
10. Shin H, Zygourakis K, Farach-Carson MC, et al. Attachment, proliferation, and migration of marrow stromal osteoblasts cultured on biomimetic hydrogels modified with an osteopontin-derived peptide. Biomaterials. 2004;25(5):895-906.
11. Rhodes NP. Inflammatory signals in the development of tissue-engineered soft tissue. Biomaterials. 2007;28(34):5131-5136.
12. Jeong B, Bae YH, Lee DS, et al. Biodegradable block copolymers as injectable drug-delivery systems. Nature. 1997;388(6645):860.
13. Zhang H, Qadeer A, Chen W. In situ gelable interpenetrating double network hydrogel formulated from binary components: thiolated chitosan and oxidized dextran. Biomacromolecules. 2011;12(5):1428-1437.
14. Tseng TC, Tao L, Hsieh FY, et al. An injectable, self-healing hydrogel to repair the central nervous system. Adv Mater. 2015;27(23):3518-3524.
15. Yang B, Zhang Y, Zhang X, et al. Facilely prepared inexpensive and biocompatible self-healing hydrogel: a new injectable cell therapy carrier. Polym Chem. 2012;3(12):3235-3238.
16. Hou S, Wang X, Park S, et al. Rapid Self-Integrating, Injectable Hydrogel for Tissue Complex Regeneration. Adv Healthc Mater. 2015;4(10):1491-1495.
17. Wei Z, Yang JH, Liu ZQ, et al. Novel Biocompatible Polysaccharide-Based Self-Healing Hydrogel. Adv Funct Mater. 2015;25(9):1352-1359.
18. Taylor DL. Self-Healing Hydrogels. Adv Mater. 2016;28:9060-9093.

19. Li Y, Zhang Y, Shi F, et al. Modulus-regulated 3D-cell proliferation in an injectable self-healing hydrogel. Colloids Surf B Biointerfaces. 2017;149:168-173.
20. Wang Y, Li L, Kotsuchibashi Y, et al. Self-Healing and Injectable Shear Thinning Hydrogels Based on Dynamic Oxaborole-Diol Covalent Cross-Linking. ACS Biomater Sci. 2016;2(12):2315-2323.
21. Ouyang L, Highley CB, Rodell CB, et al. 3D printing of shear-thinning hyaluronic acid hydrogels with secondary cross-linking. ACS Biomater Sci. 2016;2(10):1743-1751.
22. Lee KY, Ha WS, Park WH. Blood compatibility and biodegradability of partially N-acylated chitosan derivatives. Biomaterials. 1995;16(16):1211-1216.
23. Sogias IA, Williams AC, Khutoryanskiy VV. Why is chitosan mucoadhesive? Biomacromolecules. 2008;9(7):1837-1842.
24. Mourya V, Inamdar NN. Chitosan-modifications and applications: opportunities galore. React Funct Polym. 2008;68(6):1013-1051.
25. Knight DK, Shapka SN, Amsden BG. Structure, depolymerization, and cytocompatibility evaluation of glycol chitosan. J Biomed Mater Res A. 2007;83(3):787-798.
26. Park H, Kim SW, Lee JW, et al. Injectable hydrogels prepared from partially oxidized hyaluronate and glycol chitosan for chondrocyte encapsulation. Carbohydr Polym. 2017;157:1281-1287.
27. Weng L, Chen X, Chen W. Rheological characterization of in situ crosslinkable hydrogels formulated from oxidized dextran and N-carboxyethyl chitosan. Biomacromolecules. 2007;8(4):1109-1115.

28. Ding F, Wu S, Wang S, et al. A dynamic and self-crosslinked polysaccharide hydrogel with autonomous self-healing ability. Soft Matter. 2015;11(20):3971-3976.
29. Tan H, Chu CR, Payne KA, et al. Injectable in situ forming biodegradable chitosan–hyaluronic acid based hydrogels for cartilage tissue engineering. Biomaterials. 2009;30(13):2499-2506.
30. Balakrishnan B, Soman D, Payanam U, et al. A novel injectable tissue adhesive based on oxidized dextran and chitosan. Acta Biomater. 2017;53:343-354.
31. Xin Y, Yuan J. Schiff's base as a stimuli-responsive linker in polymer chemistry. Polym Chem. 2012;3(11):3045-3055.
32. Weng L, Romanov A, Rooney J, et al. Non-cytotoxic, in situ gelable hydrogels composed of N-carboxyethyl chitosan and oxidized dextran. Biomaterials. 2008;29(29):3905-3913.
33. Zhao X, Li P, Guo B, et al. Antibacterial and conductive injectable hydrogels based on quaternized chitosan-graft-polyaniline/oxidized dextran for tissue engineering. Acta Biomater. 2015;26:236-248.
34. Martínez-Sanz E, Ossipov DA, Hilborn J, et al. Bone reservoir: injectable hyaluronic acid hydrogel for minimal invasive bone augmentation. J Control Release. 2011;152(2):232-240.
35. Epstein-Barash H, Stefanescu CF, Kohane DS. An in situ cross-linking hybrid hydrogel for controlled release of proteins. Acta Biomater. 2012;8(5):1703-1709.
36. Naddaf A, Tsibranska I, Bart H-J. Kinetics of BSA release from poly (N-isopropylacrylamide) hydrogels. Chemical Engineering and Processing: Process Intensification. 2010;49(6):581-588.

37. Shi L, Han Y, Hilborn J, et al. “Smart” drug loaded nanoparticle delivery from a self-healing hydrogel enabled by dynamic magnesium–biopolymer chemistry. Chem Commun. 2016;52(74):11151-11154.
38. Gačanin J, Kovtun A, Fischer S, et al. Spatiotemporally Controlled Release of Rho-Inhibiting C3 Toxin from a Protein–DNA Hybrid Hydrogel for Targeted Inhibition of Osteoclast Formation and Activity. Adv Healthc Mater. 2017:1700392.
39. Wei Z, Zhao J, Chen YM, et al. Self-healing polysaccharide-based hydrogels as injectable carriers for neural stem cells. Sci Rep. 2016;6:37841.
40. Aziz MA, Cabral JD, Brooks HJ, et al. Antimicrobial properties of a chitosan dextran-based hydrogel for surgical use. Antimicrob Agents Chemother. 2012;56(1):280-287.
41. Lü S, Liu M, Ni B. An injectable oxidized carboxymethylcellulose/N-succinyl-chitosan hydrogel system for protein delivery. Chem Eng J. 2010;160(2):779-787.
42. Yan Y, Li M, Yang D, et al. Construction of injectable double-network hydrogels for cell delivery. Biomacromolecules. 2017;18(7):2128-2138.
43. Baker RW. Controlled release of biologically active agents. New York, NW: John Wiley & Sons; 1987.
44. Ritger PL, Peppas NA. A simple equation for description of solute release I. Fickian and non-fickian release from non-swellable devices in the form of slabs, spheres, cylinders or discs. Journal of Controlled Release. 1987;5(1):23-36.
45. Cheng Y, Nada AA, Valmikinathan CM, et al. In situ gelling polysaccharide-based hydrogel for cell and drug delivery in tissue engineering. J Appl Polym Sci. 2014;131(4).

Table 1. Gelation time of Odex/GC hydrogels

Hydrogel Sample	Polymer concentration (wt%)	Gelation time (s)
Odex/GC 1	1.0	231 ± 10
Odex/GC 2	2.0	114 ± 4
Odex/GC 3	3.0	42 ± 3

[a]The gelation times of the Odex/GC hydrogels with various polymer concentration were determined by vial invert method.

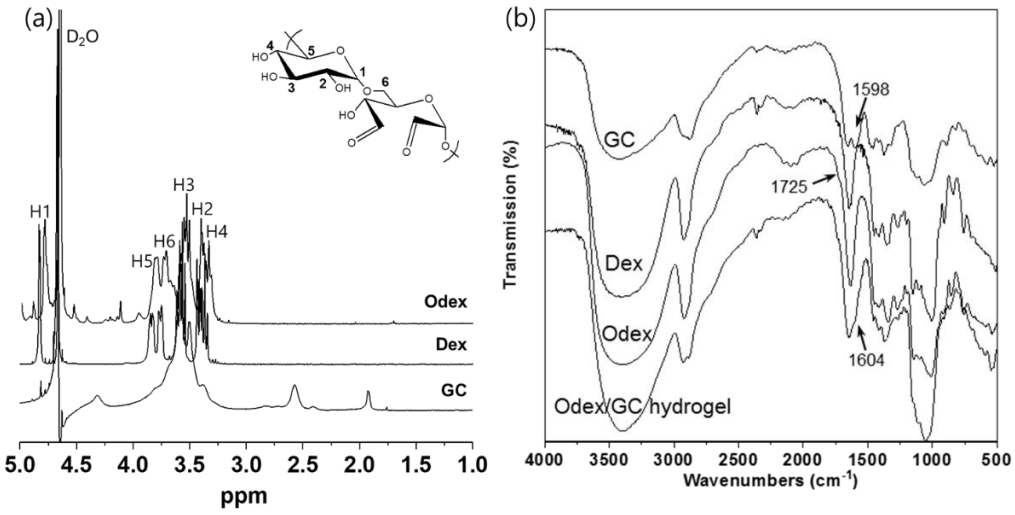

Figure 1. (a) ^{1}H-NMR spectra of GC, Dex, Odex, and (b) FT-IR spectra of GC, Dex, Odex and Odex GC hydrogel.

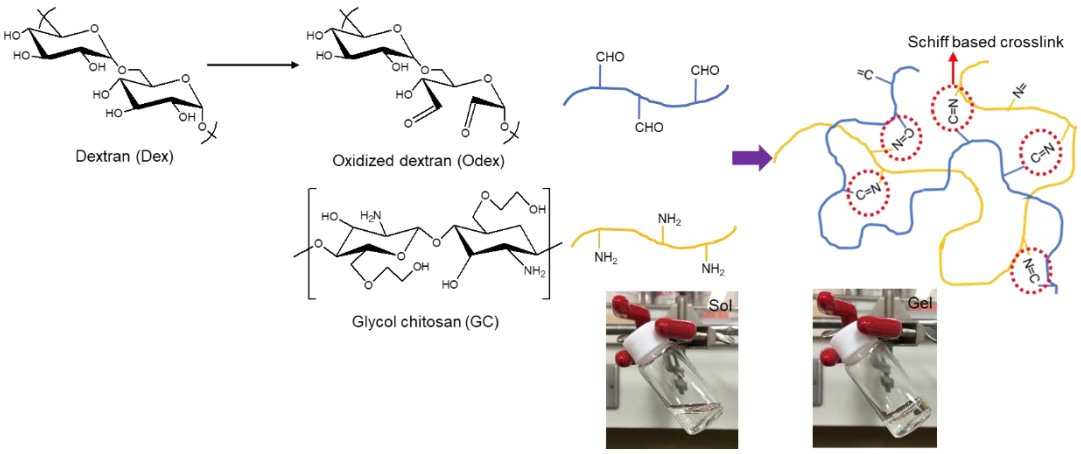

Figure 2. Synthesis scheme of periodate oxidation of dextran and hydrogel formation mechanism via the Schiff-base linkage with glycol chitosan.

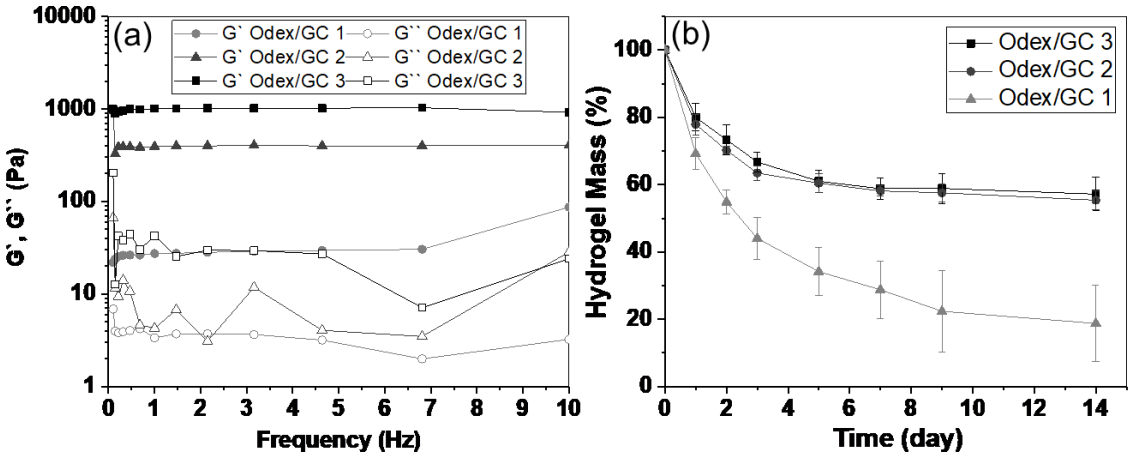

Figure 3. (a) Mechanical properties of the Odex/GC hydrogels. (b) Degradation profile of Odex/GC hydrogels in PBS at 37 ºC.

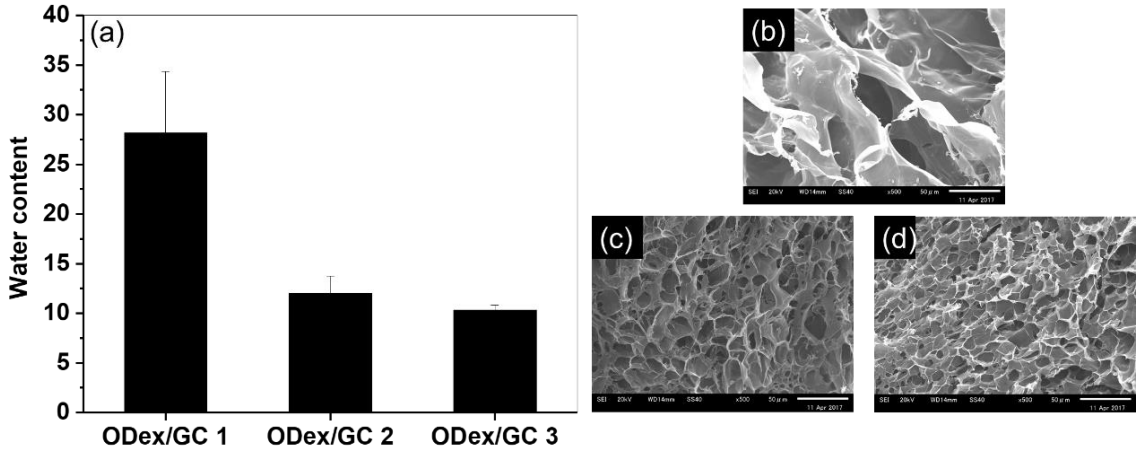

Figure 4. (a) Water content of Odex/GC hydrogels. Cross-sectional SEM images of Odex/GC hydrogels (b) Odex/GC 1, (c) Odex/GC 2, and (d) Odex/GC 3. Scale bar 50 μm.

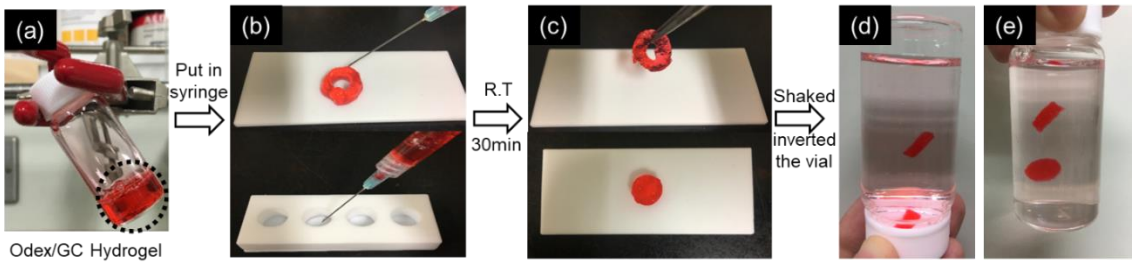

Figure 5. The injectable process of the self-healing Odex/GC hydrogel. (a) The Odex/GC 2 hydrogel was stained with red dye and (b) hydrogel was loaded into a syringe and made into a donut shape or injected into a cylindrical teflon mold. (c) The hydrogel fragments were convert into donut or cylindrical hydrogel after 30min at room temperature without any other intervention. (d, e) The self-healed hydrogels show good stability when inverted or shaken in distilled water.

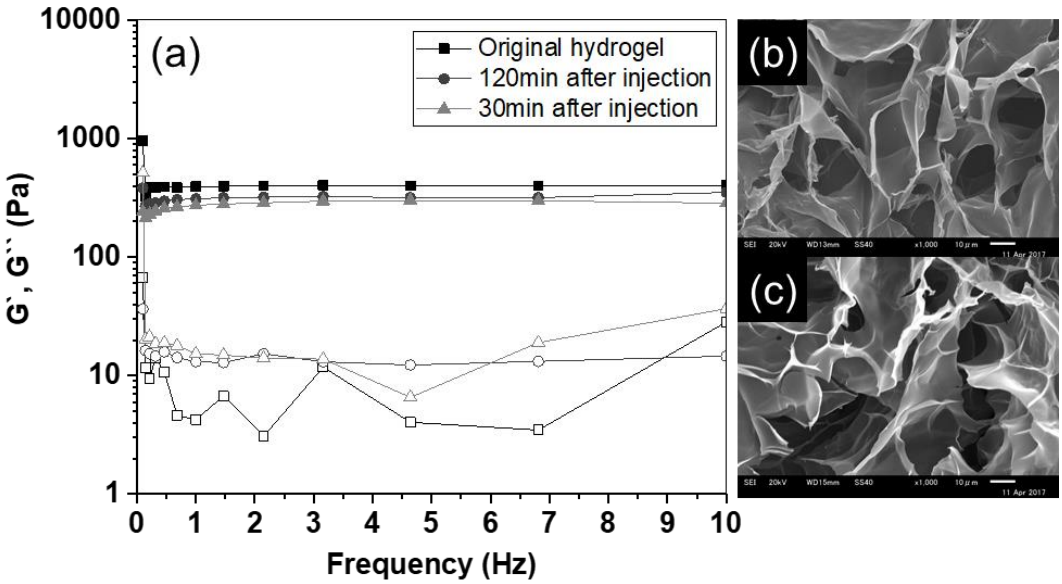

Figure 6. The rheological measurement and SEM image of self-healing Odex/GC 2 hydrogel. (a) Storage modulus G` and loss modulus G`` of the original hydrogel and the self-healed hydrogel injected after 30 and 120min. Cross-sectional SEM image of (b) original hydrogel and (c) self-healed hydrogel injected after 30min. Scale bar 10μm.

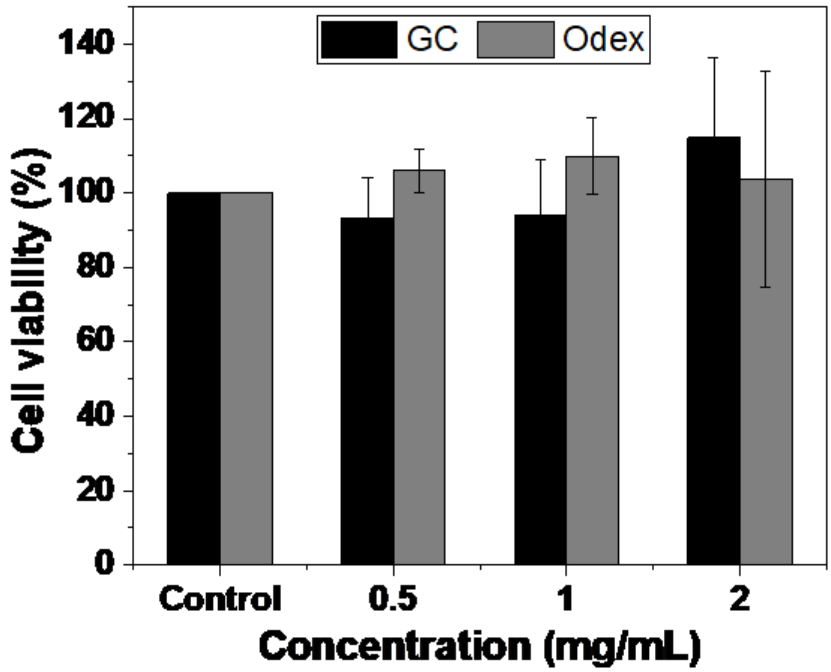

Figure 7. *In vitro* cytotoxicity study of GC and Odex to observe cell viability as a function of NIH 3T3 fibroblast. The cells were incubated with various concentration of GC and Odex (0.5, 1.0, 2.0 mg/mL), the cells were incubated for 1 day at 37 ^{o}C. As a control, 0.01M PBS (pH 7.4) was added to the cell culture medium instead of GC and Odex.

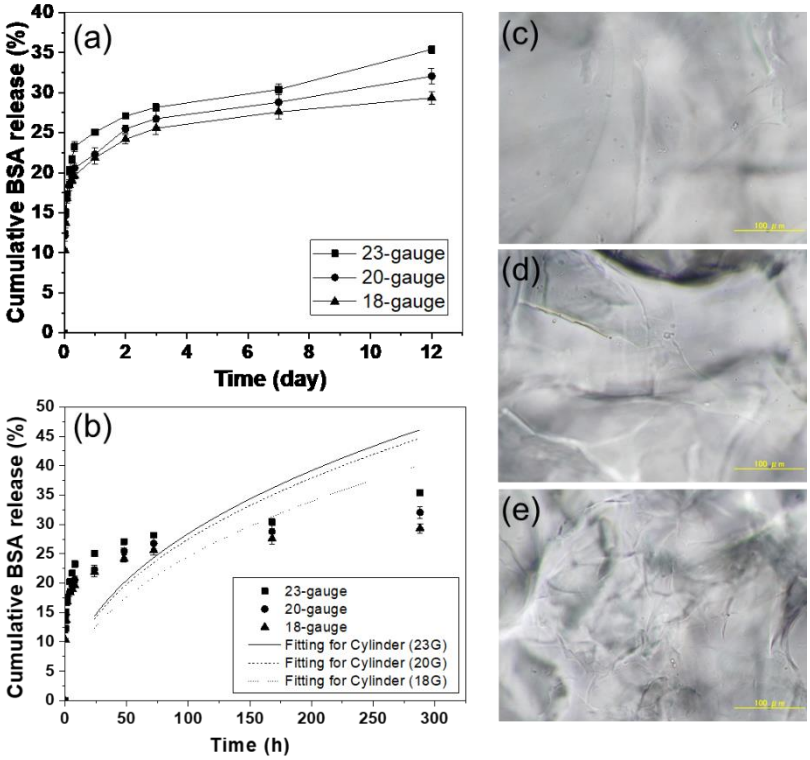

Figure 8. Release profiles of BSA from hydrogels in PBS at 37ºC. (a) cumulative BSA released from hydrogels in 12 days; (b) Curve fitting of the release profiles by the cylinder-shaped monolithic solution using equation (3) (see in the text); (c-e) microscopy images of injectable self-healing hydrogel by using (c) 18-gauge (GEL-18G), (d) 20-gauge (GEL-20G), and (e) 23-gauge needle (GEL-23G). Scale bar 100μm.